УДК 004.942 + 004.932.2

CELLULAR AUTOMATA APPROACH TO INVESTIGATION OF HIGH BURN-UP STRUCTURES IN NUCLEAR REACTOR FUEL

E. P. Akishina, V. V. Ivanov, B. F. Kostenko

Joint Institute for Nuclear Research, Dubna

Micrographs of uranium dioxide (UO_2) corresponding to exposure times in reactor during 323, 953, 971, 1266 and 1642 full power days were investigated. The micrographs were converted into digital files isomorphous to cellular automata (CA) checkerboards. Such a representation of the fuel structure provides efficient tools for its dynamics simulation in terms of primary «entities» imprinted in the micrographs. Besides, it also ensures a possibility of very effective micrograph processing by CA means. Interconnection between the description of fuel burn-up development and some exactly soluble models is ascertained. Evidences for existence of self-organization in the fuel at high burn-ups were established. The fractal dimension of microstructures is found to be an important characteristic describing the degree of radiation destructions.

Исследуются микрофотографии диоксида урана (UO_2), отвечающие времени пребывания в реакторе с полной рабочей нагрузкой в течение 323, 953, 971, 1266 и 1642 сут. Микрофотографии были преобразованы в цифровые файлы, изоморфные рабочему полю клеточного автомата (КА). Такое представление позволяет моделировать динамику структур в топливе в терминах самих элементов изображения, представленных на микрофотографиях. Кроме того, это представление микрофотографий обеспечивает возможность их эффективной обработки средствами КА. Установлена связь между описанием динамики выгорания топлива и некоторыми точно решаемыми моделями. Получены указания на то, что процесс выгорания, начиная с некоторого порогового значения степени выгорания, протекает самоорганизующимся образом. Показано, что фрактальная размерность микроструктур в топливе является важной характеристикой, описывающей степень его разрушения в процессе выгорания.

INTRODUCTION

Formation of high burn-up structures in UO_2 nuclear fuel materials, known as *rim effect*, attracts attention mainly due to its possible catastrophic influence on the operation conditions of modern nuclear power stations. This process, resulting in the gross structural damage, polygonization or grain subdivision, is of big scientific interest as well, because physical mechanisms and relevant parameters of it are still poorly understood. As a huge amount of interacting particles take part in the process, the underlying dynamics may have essentially a nonlinear chaotic behavior giving rise to fractal structures. In this paper, we examine a new way of investigating the burn-up structure formation based on CA. Some more details on this subject have been published in our previous papers [1–6].

We investigated the UO_2 fuels with average cross section burn-ups 16.2, 42.6, 43.9, 54.8 and 65.0 GWd/tM corresponding to exposure times in reactor during 323, 953, 971, 1266 and 1642 full power days, respectively. The micrographs with magnification of 1250 times of the

material surface subjected to both «as-polished» and «as-etched» conditions were considered. As a rule, the micrographs corresponding to the «as-polished» surface are usually required to observe fission gas (mainly Kr and Xe) bubbles and evaluate the porosity of the material. Micrographs of the «as-etched» surface are useful for visualization of the grain-boundaries and cracks which become visible due to preferential attack of the acid on pre-stressed points of the sample, as, e.g., those showing accumulation of dislocations near grain and subgrain boundaries.

The next Section describes preparing digital images from optical micrographs. CA basic concept relevant to this study is briefly sketched in Sec. 2. The results of CA image processing and some physical inferences from them are presented in Secs. 3–6. Section 7 is devoted to fractal analysis of high burn-up structures. We demonstrate capabilities of CA to reproduce the rim structure dynamics in Secs. 8 and 9 using a pore formation and an etching process as characteristic examples. Some perspectives of possible further development of CA approach to the rim structure investigation are summarized in Conclusion.

1. PREPARATION OF DIGITAL IMAGES

After scanning, the micrographs were transformed to visual files in TIF format and cut into pieces of 1200×500 pixel size. In turn, these images were transformed with Photoshop into black-and-white ones by gradually adjusting the brightness and contrast. One can estimate the quality of the latter transformation by comparing Figs. 1 and 2.
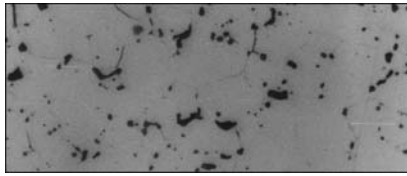

Fig. 1. The scanned micrograph corresponding to the «as-polished» pattern at 16.2 GWd/tM burn-up
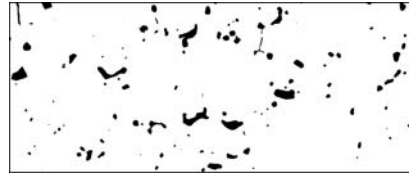

Fig. 2. Black-and-white transformation of Fig. 1

The obtained images were converted into digital (ASCII) files so that the smallest black and white cells in the computer screen were represented by 0 and 1, correspondingly. The final digital files are nothing else but CA checkerboards which are completely prepared for CA data processing. In the subsequent sections we consider some results of this treatment; corresponding algorithms and programs are described elsewhere [3].

2. CELLULAR AUTOMATON BASIC CONCEPT

CA were introduced in 1948 by von Neumann for explanation of complex living processes in terms of the dynamics of many identical simple cells capable of interacting maintaining their individuality. The game «Life» invented by John Conway in 1970 is a famous example

of such a type. Today CA are not only useful in theoretical biology [7], but they provide an effective practical tool for theoretical investigations of many other cooperative effects in complex systems in cases their components follow simple local rules. In particular, the models of statistical mechanics, which operate on a regular lattice with local interactions between sites (such as models of percolation, nucleation, condensation, coagulation, lattice spin models, etc.), «are begged for cellular-automaton simulation» [8]. Now CA successfully compete with continuum models of reality in the form of differential equations in all cases the discreteness is an intrinsic feature of the physical system (like in crystals), or where continuum models meet serious difficulties and discrete formulations are needed as a regularization (like in lattice-gauge field theories [9]), or as an effective approximation (e.g., lattice-gas molecular dynamics [10]). There are also very effective applications of CA to processing of digital images of complex extended objects. For all the above reasons we try here employing CA for investigation of the burn-up structure formation in UO_2.

Standard Cellular Automaton is a simple dynamical system, the behavior of which is defined by local relations between its units or «cells». Schematically CA can be presented as a periodic space grid that is constructed and performed in accordance with the following algorithm:

1. Cells and their possible discrete states are defined; usually each cell may assume one of two states, 0 or 1 (however, there may be cellular automata with more states).

2. Interconnections between cells are defined; as a rule, each cell can only communicate with neighbor cells. The neighborhood, for the lattice consisting of squares, may be understood in the von Neumann or Moore sense. In the first case only the nearest Northern (N), Southern (S), Westerly (W) and Easterly (E) neighbors are taken into account. In the Moore neighborhood the four other neighbors which touch a central cell at the NW, NE, SW and SE sides are considered additionally (see Fig. 3).
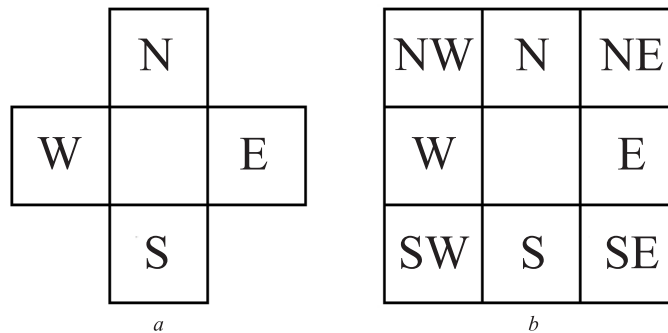
Fig. 3. The von Neumann (*a*) and Moore (*b*) neighborhoods

3. Rules determining evolution of the cellular automata are fixed. A state of each cell is updated according to the fixed transition rules, which are determined by the actual problem considered and usually have a simple functional form; the result of the transition depends on the cell state and the states of its neighbors.

4. CA is a timed system, in which all cells change states simultaneously.

3. ESTIMATION OF SPATIAL DISORDER

The entropy function of patterns allows one to evaluate the main components of spatial disorder in the micrographs. Let us consider a local patch of four adjacent sites of the checkerboard with coordinates (i, j), $(i+1, j)$, $(i, j+1)$ and $(i+1, j+1)$. It is evident that there are $2^4 = 16$ possible black-and-white colorings for the patch. Then, the information entropy of the spatial pattern H_s at an arbitrary time t can be defined by

$$H_s(t) \equiv -\sum_k P^k(t) \log_{16} P^k(t),$$

where $P^k(t)$ is the probability for a particular coloring of the local patch at time t. The base 16 is used for log, because the entropy is assumed to take its value between 0 and 1. Typical spatial patterns of UO_2 «as-polished» surfaces at different values of burn-up at the depth from 40 to 100 μm from the surface are shown in Fig. 4, *a–d*.
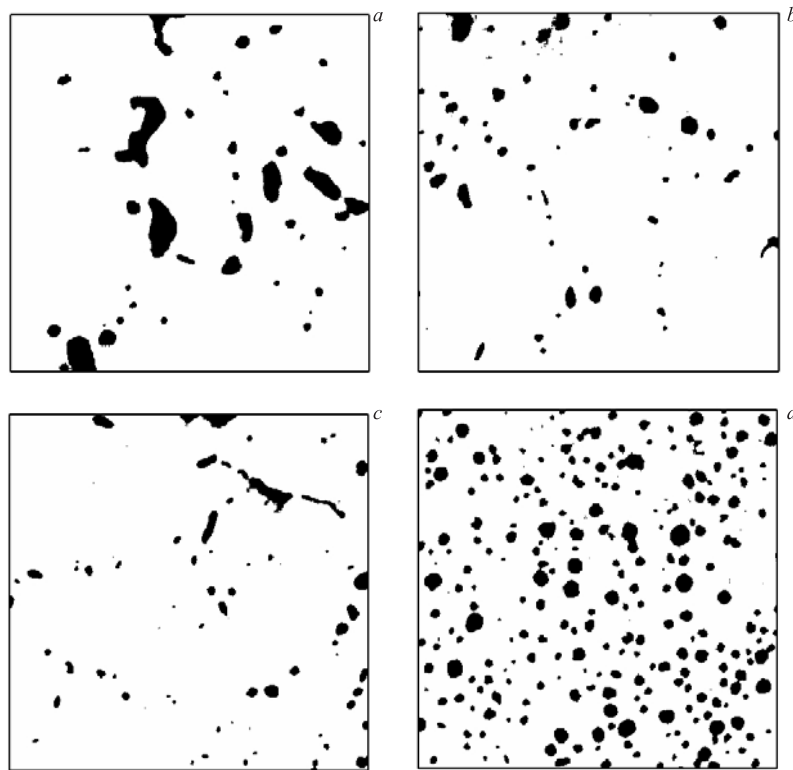

Fig. 4. Patterns of UO_2 «as-polished» surfaces at different values of burn-up: *a)* 16.2 GWd/tM; *b)* 42.6 GWd/tM; *c)* 43.9 GWd/tM; *d)* 65 GWd/tM

We have found the entropy for «as-polished» patterns for different burn-ups at the prescribed depths in the interval $40 \div 100$ μm from the surface of fuel pellets (see Table 1).

Table 1. **The information entropy and ratio of black to white areas versus burn-up (in GWd/tM) for «as-polished» micrographs**

Burn-up	16.2	42.6	43.9	54.8	65
H_s	0.146	0.106	0.104	0.155	0.301
S_b/S_w	0.075	0.038	0.037	0.059	0.159

It is possible to recognize two different causes of the spatial disorder by comparing the values of H_s in Table 1 with corresponding micrographs. The first one is rather evident. This is a «pulverization» of black cells due to diffusion of micropores into the material. The second cause can be the growth of the total number of black cells in the micrographs. Indeed, maximum of the entropy corresponds to equal numbers of black and white cells, but in micrographs the black cells are always in minority.

4. THERMODYNAMICS OF BUBBLE'S VOLUME

In connection with the third row of Table 1, a question arises about the reason for the mean bubble's volume decrease at moderate ($16.2 \div 43.9$) burn-ups and its increase at high ($54.8 \div 65$) ones. Here we give explanation for this in the framework of a thermodynamic model (information entropy, mentioned above, should not be confused with the thermodynamic entropy encountered below).

Let us consider a system of two different substances (uranium dioxide, *substance 1*, and its fission products, *substance 2*), which form two adjacent phases (gaseous, *phase I*, and solid, *phase II*). Then the phase equilibrium implies

$$\mu_1^{\mathrm{I}}(P,T,c^{\mathrm{I}}) = \mu_1^{\mathrm{II}}(P,T,c^{\mathrm{II}}),$$

$$\mu_2^{\mathrm{I}}(P,T,c^{\mathrm{I}}) = \mu_2^{\mathrm{II}}(P,T,c^{\mathrm{II}}),$$

where T and P are the common temperature and pressure in the phases; μ is the chemical potential, and c is the concentration. Any infinitesimal change of the system temperature or pressure induces the chemical potential change in the form

$$d\mu^i = -s^i\, dT\ +\ v^i dP, \tag{1}$$

where s^i and v^i are the entropy and volume per molecule for the gaseous ($i = \mathrm{I}$) and the solid ($i = \mathrm{II}$) phases. As far as

$$s^{\mathrm{I}} \neq s^{\mathrm{II}}, \qquad v^{\mathrm{I}} \neq v^{\mathrm{II}},$$

the infinitesimal change in temperature and pressure leads to the breakdown of the system equilibrium. One can evaluate the direction of processes which will occur afterwards during the system's return to equilibrium. Since for evaporation of the matter from the solid, the heat $dQ = T\, dS$ must be absorbed, i.e., $dQ > 0$, the inequality

$$s_i^{\mathrm{I}} > s_i^{\mathrm{II}}$$

must be satisfied.

Therefore, if the temperature increases (at constant P), the chemical potential for the gaseous phase becomes, in accordance with Eq. (1), lower than its value in the solid phase. For equilibrium restoration, the vapor begins to enter into bubbles from the solid, and the balance will be restored (as far as $(d\mu/dn)_{P,T} > 0$). This process is very probable to take place at high burn-up (see Table 1), where temperature increase is expected, in particular, due to lowering of the thermoconductivity of the destroyed matter.

It is also possible to show [1] that

$$v_i^{\mathrm{I}} > v_i^{\mathrm{II}}.$$

Therefore, the infinitesimal increase of P at constant T leads, in accordance with (1), to a tiny increase of the difference $\delta\mu = \mu_i^{\mathrm{I}} - \mu_i^{\mathrm{II}} > 0$. To restore the thermodynamic equilibrium, the substances will condensate from the gaseous phase into the solid one. This process can be responsible for dissolution of big irregular bubbles and decrease of the total bubbles' volume which are seen in the micrographs at early and middle stages of fuel evolution.

5. FLUCTUATIONS OF BLACK CELL QUANTITY

The question «Are large parts of the micrographs statistically independent, as it is usually the case for macroscopic parts of the thermodynamic system in equilibrium?» is very important to reveal the true nature of processes seen in the micrographs. If the answer is affirmative, one can describe the «large part» of the micrograph using some kind of the Gibbs distribution. Otherwise, cooperative processes, which are characteristic for nonlinear self-organizing phenomena, are expected to take place.

Before giving answer to this question, one has to decide firstly what the minimal size of the checkerboard could be considered as «large». It is well known that statistical ensembles, even consisting of moderate numbers of particles, merely several hundred, often demonstrate properties inherent in the macroscopic system. Another crucial point is the requirement for the subsystem to interact weakly with the rest part of the whole system. If we suppose that interactions between different parts of the system do not range further than to one pixel in the checkerboard, then the following upper bound for the ratio of the surface energy to internal one, E_s/E_{in}, for any fragment of the checkerboard can be obtained:

$$E_s/E_{\mathrm{in}} = N_s/N_{\mathrm{in}},$$

where N_s and N_{in} are the numbers of the lattice links on the fragment surface and in the interior, correspondingly. For example, for a 40×40 square, the ratio is equal to

$$\frac{E_s}{E_{\mathrm{in}}} = \frac{4 \cdot 40}{39 \cdot 39} \approx \frac{1}{10}$$

and can be treated as a small number. Therefore, squares containing 40×40 pixels included in a complex fragment of a micrograph (800×800 pixels) were chosen as «large» enough and weakly interacting with surrounding cells. In Fig. 5, we show the complex fragment of a micrograph containing 800×800 pixels. A small square (40×40 pixels) denotes a typical size of the subsystem which we consider as a «large» one and weakly interacting with surrounding cells.

To calculate the total number, N, of black cells and the length, L, of boundary between the black and white regions in it, a special cellular automaton («land surveyor») has been elaborated [3]. The distributions found (see [1]) do not resemble the Gibbs one:

$$w_{L,N} = A \exp\left(\mu N - E_{L,N}\right)/kT,$$

where μ is the chemical potential and $E_{L,N}$ the energy of the subsystem which is expected to be a monotone function of L and N. We consider this fact as a hint at the possible self-organizing nature of the process.

Fig. 5. Pattern used in this study

Remark: Nevertheless, we cannot still exclude Gibbs distribution applicability for bubble fluctuation description, if some other, more relevant thermodynamic variables, will be chosen. In particular, one can consider as statistically independent the characteristics of each *separate* bubble, for which the following distribution of the total boundary length fluctuation of i bubbles in the «large» subsystem can be deduced: $w_i(L) = \int_0^\infty dL_1 \ldots \int_0^\infty dL_i w_1(L_1) \ldots w_1(L_i)\delta(L_1 + \ldots + L_i - L) \simeq CL^{i-1}\,\mathrm{e}^{-L/kT}$. Here L_k are boundary lengths of individual bubbles, $w_1(L_k) = 1/kT \exp\left(-L_k/kT\right)$. Such a distribution is quite consistent with «land surveyor» observations. A more realistic physical description should also include the value S of 2-dimensional boundary instead of L and take into account compressibility of gas in bubbles instead of plain count of numbers of black cells in them.
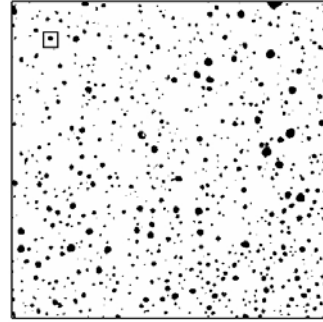
6. ON SIMILARITY BETWEEN UO$_2$ AND LIQUID

It is interesting to find direct evidence for such a commonly accepted assumption that fission gas bubbles in UO$_2$ (a ceramic with melting point of 2880 °C) behave very similarly to usual bubbles in the liquid, in particular, to verify an assumption that bubble gas pressure and tension of the bubble surface have an influence on the statistical distributions of bubble sizes. Accurate quantitative investigations of these effects could give another means to ascertain if the thermodynamic equilibrium is settled in the bubbles' vicinity or not. For this purpose, we have investigated a more delicate characteristic — a two-hillock behavior of the distributions seen in Fig. 6. To reveal this property, a «Black Cell Eater» cellular automaton (BCEA) was designed [3]. For interpretation of this histogram, we suggest that the separation surface between gaseous and solid phases is controlled by a requirement for it to have the smallest possible value for the effective volume of the gaseous phase to be fixed:
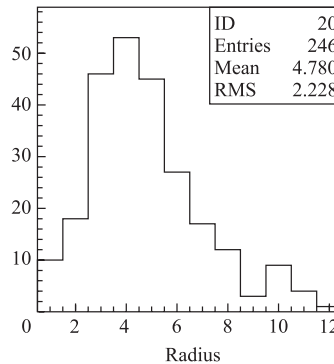
Fig. 6. Pore radii distribution at 65 GWd/tM

$$\alpha\, 4\pi r_1^2 + 4\pi r_2^2 = \min, \tag{2}$$

$$\alpha\,\frac{4\pi r_1^3}{3} + 2\frac{4\pi r_2^3}{3} = \text{const.} \tag{3}$$

Here α is a ratio of the number of big and small pores, correspondingly, seen on the surface of a pattern. The factor 2 in Eq. (3) means that infinitesimal volume transfer from a small pore to a big one is accompanied with double increase of its value (as far as the ratio of the pressures inside the two pores is inversely proportional to the ratio of their radii).

One can easily solve the system (2), (3) and find

$$r_1 = 2r_2.$$

Thus, the data obtained with BCEA indeed appears to be in agreement with the assumption that surface tension and compressibility of gas in bubbles play the crucial role in pore formation process.

7. FRACTAL ANALYSIS

In order to get additional information on a mechanism of the phenomenon, we analyzed optical micrographs of the rim-zone of various liquid water reactor fuels applying fractal analysis methods [2]. Our conclusion that the images on micrographs are of fractal character is based on results of numerical calculations of the length corresponding to the boundaries between black and white features, showing a power-law dependence with a characteristic length δ. By calculating the number $N(\delta)$ of elements, such as squares or circles with a characteristic length δ, necessary to cover the boundaries, one gets their approximate length

$$L(\delta) = a\delta^{1-D}, \tag{4}$$

where $a = L_0$ is a constant corresponding to small δ, and D is the fractal dimension, which is equal to 1 for the smooth line. Taking into account that $L(\delta) = N(\delta)\delta$ and making use of Eq. (4), one gets

$$\ln N(\delta) = \ln a - D\ln\delta. \tag{5}$$

By changing the characteristic length δ from minimal value up to a reasonable maximal value, we determine the slope D.

For the computation of the fractal dimensions of the micrographs we used two recently developed software packages, namely, PLATO from the Laboratory of Information Technologies of the Joint Institute for Nuclear Research [11] and BIP from the University of Memphis [12]. The package PLATO is based on a box-counting algorithm, while the package BIP includes 11 different methods. An example of BIP usage is shown in Fig. 7.

The procedure of the micrograph image processing consisted in the following. All graphical files (rasters), prepared from micrographs after their scanning with resolution 150 dpi, were saved as BMP-files in A4 format. Then, the central part of each raster of fixed size $(62.5 \times 126.5\,\mu\text{m})$, corresponding to the best quality of the image, was extracted and corrected using brightness and contrast options of the Adobe Photoshop. The brightness was increased up to 80% and the contrast was fixed. Rasters prepared in such a way for the «as-etched» micrographs were reliable enough for their effective processing without any additional image corrections with the BIP tools. On the contrary, the rasters of the «as-polished» samples
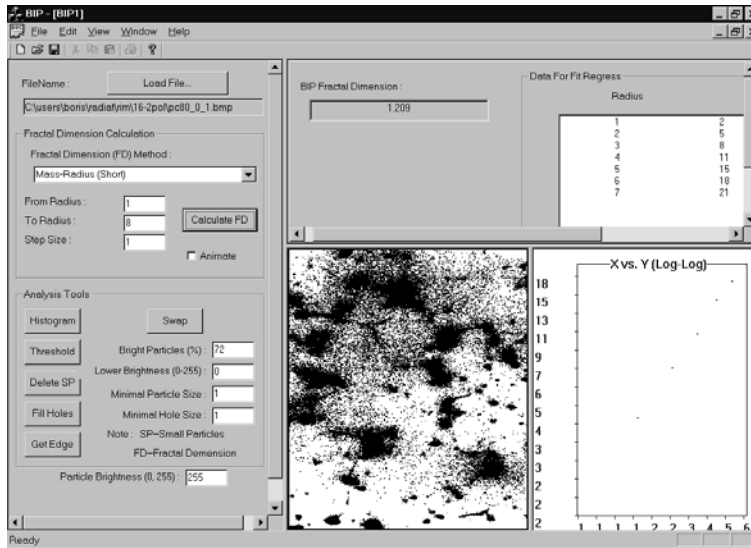
Fig. 7. The artificial «etching» by tools of the BIP code of 16.2 GWd/tM «as-polished» sample. The adjustment parameters as well as the calculation results are also presented

needed additional corrections with the BIP tools. Namely, it was necessary to apply additional corrections of the brightness and contrast, in order to reveal the pore image features. This procedure played the role of an artificial «etching» of the «as-polished» samples. Of course, contrary to real chemical etching, such image corrections do not reveal any cracks. The increase of contrast in BIP was achieved by setting a portion of bright «particles» equal to 72%.

Table 2. **Fractal dimensions for «as-polished» micrographs. Non rim-transformed material:** $D >$ 1.14**. Rim-transformed material (self-organization):** $D \leqslant 1.14$

Fractal dimension	Fuel average burn-up, GWd/tM			
	16.2	43.9	54.8	65
D_1 (pellet edge)	1.21	1.35	**0.98**	**1.05**
D_2 (150–200 μm from pellet edge)	1.51	1.32	1.49	**1.14**
$\langle D \rangle$ (average at 0–200 μm from edge)	1.36	1.34	1.24	**1.10**

In Table 2 we present the results of the computation of the fractal dimension D for the «as-polished» micrograph images, which were preliminarily «etched» using the tools of the BIP code. Hereafter, D_1 is the fractal dimension for the micrograph regions close to the sample's surface, and D_2 for the region at 150 to 200 μm radial depth from the surface. For the computation of the fractal dimension we mainly used the «mass-radius» algorithm: the value of the radius changes from 1 pixel up to the maximal value of 8 to 10 pixels with a step of 1 pixel. From Table 2 one can see that the fractal dimension decreases for a given

burn-up as one approaches the sample's surface from the pellet center. On the other hand, the fractal dimension decreases as the burn-up increases.

Table 3 shows the results obtained for the «as-etched» micrographs under the same conditions by applying the same computational algorithm (we remind that these images were not corrected with the BIP tools).

Table 3. **Fractal dimensions for «as-etched» micrographs. Non rim-transformed material:** $D >$ 1.18**. Rim-transformed material (self-organization):** $D \leqslant 1.18$

Fractal dimension	Fuel average burn-up, GWd/tM			
	16.2	43.9	54.8	65
D_1 (pellet edge)	1.34	**1.14**	**1.06**	**1.17**
D_2 (150–200 μm from pellet edge)	1.40	1.24	1.24	**1.08**
$\langle D \rangle$ (average at 0–200 μm from edge)	1.37	**1.18**	**1.15**	**1.13**

The comparison of Tables 2 and 3 shows the validity of our general conclusion that the fractal dimension decreases as the burn-up increases, although the fractal dimensions calculated for «as-etched» and «as-polished» surfaces are different.

Table 4. **Fractal dimensions for «as-etched» micrographs. Non rim-transformed material:** $D >$ 1.20**. Rim-transformed material (self-organization):** $D \leqslant 1.20$

Fractal dimension	Fuel average burn-up, GWd/tM			
	16.2	43.9	54.8	65
D_1 (pellet edge)	1.267	**1.142**	**1.025**	**1.029**
D_2 (150–200 μm from pellet edge)	1.274	1.213	1.207	1.208
$\langle D \rangle$ (average at 0–200 μm from edge)	1.271	**1.178**	**1.116**	**1.119**

In Table 4 we present the fractal dimensions for «as-etched» samples calculated applying the Euclidean Distance Map (EDM) method. They are in qualitative agreement with Table 3. Note that the transition between the non-restructured (non-rim) and restructured (rim) fuel regions, assumed respectively as non-organized and self-organized microstructures, was set at the burn-ups where the steepest decrease of the D_1, D_2 and $\langle D \rangle$ values occurred. For each micrograph condition, e.g., «as-polished», «as-etched» and «as-etched»-EDM, a respective, unique, D-transition value was assigned, as the largest of the individual transition values observed in the parameters D_1, D_2 and $\langle D \rangle$ for each micrograph condition, which is remarked at the bottom of the tables.

In agreement with the nature of the rim-process, namely, progressing from the pellet edge towards the pellet center, the fractal «non-rim/rim» transition is detected first (i.e., at lower burn-ups) in the D_1 values, as they apply to the outermost fuel regions. Furthermore, the transition appears to be detected first (i.e., also at lower burn-ups) in the «as-etched» micrographs, as they consider modifications of both porosity and grain boundary features. As remarked in the literature of the rim-process, the rim transition implies synergistic reorganization of both porosity and grain structures [14, 15]. Therefore, considering the transition (i.e., abrupt decrease) of the D_1 values of the «as-etched» micrographs as primary indication of

the rim-structure onset, the present study reveals this transformation for edge pellet regions already in the fuel with 43.9 GWd/tM average burn-up.

An evident peculiarity for the column 65 in Table 3 is worthy of notice. In this case, contrary to majority of the fuel examined, $D_2 < D_1$. However, since the general trend $D_2 > D_1$ is consistent with the main characteristic of the rim phenomenon indicating a higher degree of transformation (self-organization) towards the fuel periphery [16], the inversion of the D-trend in the particular case (with $\Delta D/D < 8\%$) might be attributed to the statistical reasons.

8. DYNAMICS OF BUBBLE VOLUME

Establishment of deterministic equations describing evolution of individual bubbles is hardly possible now because of difficulty of taking micrographs for the same pattern at different instants of time. At these circumstances (and because the evolution could be stochastic in principle), one can hope to ascertain only some probabilistic equations describing temporal development of the pattern visual characteristics with the burn-up increase and, thus, transforming in some *statistical sense* one micrograph into another.

Using CA processing, we single out the following peculiarities of this dynamics:

1. Evolution from 16.2 to 42.6 GWd/tM is accompanied with: a) dissolution of very big non-spherical bubbles (see Sec. 3); b) growth of spherical bubbles; c) birth of new very small spherical bubbles.

2. Transition from 42.6 to 54.8 GWd/tM: a) very big non-spherical bubbles totally disappeared; b) no noticeable changes in the dynamics of spherical bubbles.

3. A drastic change of evolution for $54.8 \rightarrow 65.0$ GWd/tM transition; namely: a) very quick growth of bubble's volume; b) disappearance of very small bubbles.

The last stage of evolution looks as a sudden eruption of fission gas products into pores from surrounding matrix (see Sec. 3). Besides, one cannot exclude the existence of bubble *coalescence*.

In the framework of a simple model, which ignores the total volume increase accompanying the bubble coalescence, bubble-fuel mixture can be treated as a binary alloy made up of atoms of two types. Let $\varepsilon_{\mathrm{bb}}$ and $\varepsilon_{\mathrm{ww}}$ be the interaction potential between neighboring black and white cells, correspondingly, and $\varepsilon_{\mathrm{bw}}$ be the interaction potential between neighboring sites of different colors. We assume the following simple type of interactions (which corresponds to black liquid spots immersed into white gaseous environment): $\varepsilon_{\mathrm{ww}} = \varepsilon_{\mathrm{bw}} = 0$, $\varepsilon_{\mathrm{bb}} < 0$. Now we ascribe to every black spot in the checkerboard the following potential energy proportional to its «surface»: $E = -\varepsilon_{\mathrm{bb}}L$, where L is the length of the spot boundary, and we assign to the white and black cells in the micrographs the values of 1 and –1. At equilibrium the probability of a black cell evaporation from the surface is determined by the Boltzmann distribution, $p = C \exp(-\beta\Delta E)$, where C is the normalizing constant and ΔE the energy increase due to a surface enlargement. It is clear that evaporation of a black cell, which has only one black neighbor, requires the energy input $\Delta E = \varepsilon_{\mathrm{bb}}$, whereas black cells with two and three black neighbors need $2\varepsilon_{\mathrm{bb}}$ and $3\varepsilon_{\mathrm{bb}}$ energy inputs, accordingly. Thus, the probability of black cell evaporation from the surface of the black spot is described by one of the following probabilities: p, p^2, p^3.

Formulas of this Section define the probabilistic *Ising cellular automaton* (ICA) which can simulate pattern evolution governed by temperature changes. Numerical experiments with ICA have shown that an initial micrograph, taken for real fuel, can be efficiently transformed into a theoretical image with either increasing (coalescing) or decreasing (evaporating) black patches (bubbles in the micrograph), depending on the temperature value [1].

9. SIMULATION OF RECOVERY AND ETCHING WITH CA

The etching can naturally be reproduced in the framework of the so-called *voter model*, which was intensively investigated from a pure mathematical point of view [13]. To demonstrate the efficiency of the CA approach to problems of this kind, we considered a voting rule that describes the process of recovery of patterns corresponding to the as-etched micrographs [1]. Figure 8 shows the as-etched pattern used for the *anti*-etching procedure simulation, and Fig. 9 demonstrates the results of its recovery (after five iterations). Simulation of etching can be also effectively fulfilled as a reverse process. For etching, except from pores, small points representing «halos» of primary defects responsible for the chemical etching around cracks should be introduced [1].
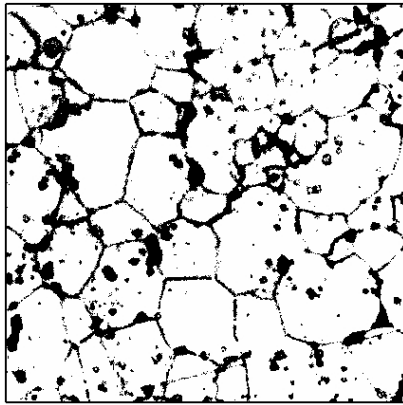

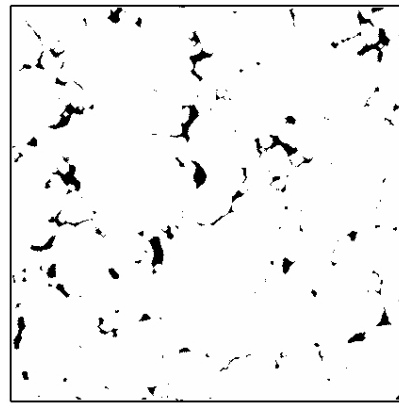Fig. 8. Initial as-etched pattern   Fig. 9. The result of *anti*-etching

CONCLUSION

In this paper we proposed a new, based on cellular automata, approach for processing and modelling the structure dynamics of nuclear reactor fuel at different burn-ups. We have shown that this approach equips us with a universal instrument applicable both to micrograph processing and to simulation of the fuel structure dynamics. Such immediate interconnection between raw experimental data and mathematical description of the process turned out to be possible only due to the fact that the micrograph image on the computer monitor is

nothing else but the CA checkerboard. Under these circumstances, one can directly formulate computer models in terms of entities imprinted in micrographs, although usage of more fundamental notions, such as energy, entropy, temperature, etc., is necessary to assign a physical interpretation to the model. Thus, CA simulation, under corresponding theoretical understanding, provides us with a moving view of the processes in the computer monitor, which one can compare with experimentally observed UO_2 micrograph evolution. This comparison may include, besides the visual one, the comparison of quantitative characteristics, which could be extracted using different CA, the same for real and theoretical images. The fruitfulness of this approach for theoretical model elaboration has been demonstrated in this work by formulation of the bubble volume thermodynamics, investigation of bubble volume fluctuations, obtaining the direct evidence for gas compressibility and bubble surface tension.

One more advantage of CA modelling is its interconnection with exactly soluble mathematical models. Such a bridge can give sometimes an additional insight into the problem. For example, the Ising model predicts a phase transition at high burn-ups, which could be hardly recognized in the framework of any purely phenomenological approach.

To be still far from the complete physical understanding of the rim structure dynamics, we believe that CA approach is a step in the right direction. Indeed, it is well known that CA simulation, to be specified at the local level, usually results in description of self-organizing global processes, resembling rim structure formation. The study undertaken in this work has revealed interesting, important for the problem of safety of modern nuclear power stations, change of bubbles dynamics at the high burn-ups. Further study of this process requires detailed CA modelling of formation of pore interconnections (intergranular channels, cracks, etc.) which could lead to some percolation threshold indicating the moment when fission gases can move through the pattern and escape outside. If such a process takes place, then modern nuclear power stations could use their fuel during much longer period of time, without a danger of explosion. This could have a serious economical effect. We believe that future complex investigations, including both CA simulation and experimental study, should shed light on this interesting interdisciplinary problem.

The numerical experiments undertaken in this work show that the fractal dimension decreases with increasing burn-up. This property remains scale invariant (we have checked it for maximal radii of covering circles of about 1, 1.6 and 2.5 μm). In addition, it is found that, on surpassing the average burn-up $\sim$ 40 GWd/tM, a pronounced decrease of the micrographs' fractal dimension at the fuel periphery occurs, as an indication of the onset of a self-organization process (rim transformation). This fairly coincides with previous OM and SEM microscopy observations in LWR-fuels, setting the onset of the rim transformation at about 40 GWd/tM [16]. The same conclusion follows from CA analysis of fluctuations, though with less reliability. Therefore, fractal dimension can turn to be an important parameter in the future theory of rim structure formation.

REFERENCES

1. *Antoniou I. et al.* Cellular Automata Study of High Burn-up Structures // Chaos, Solitons and Fractals. 2003. V. 18, No. 5. P. 1111–1128.

2. *Antoniou I. et al.* Fractal Analysis of High Burn-up Structures in UO_2 // Chaos, Solitons and Fractals. 2004. V. 19, No. 4. P. 731–737.

3. *Akishina E. P., Ivanov V. V., Kostenko B. F.* Investigation of High Burn-up Sructures in Uranium Dioxide Applying Cellular Automata: Algorithms and Codes. JINR Commun. P11-2003-184. Dubna, 2003. P. 1–40.

4. *Akishina E. P. et al.* Cellular Automata Modeling of High Burn-up Structures in UO_2 // Book of Abstr. of the V Intern. Congress on Mathematical Modelling, Sept. 30 – Oct. 6, 2002. Dubna, 2002. V. 1. P. 137; a comprehensive version in «Comput. Meth. Sci. Eng.» (in press).

5. *Antoniou I. et al.* Cellular Automata Modelling and Fractal Analysis of High Burn-up Structures in UO_2 // WSEAS Trans. Comput. 2003. V. 2. P. 1061–1066; Proc. of WSEAS Conferences: Aug., Sept., Oct., Nov. 2003.

6. *Antoniou I. et al.* Fractal Analysis of High Burn-Up Structures in UO_2 // Studies of the RIM Effect in UO_2 / Eds. I. Antoniou, V. Ivanov. SOLVAY Commun. 01–3. Brussels, 2001.

7. *Kaufmann S. A.* Emergent Properties of Random Complex Automata // Physica D. 1984. V. 10. P. 145–156.

8. *Vichniac G. Y.* Simulating Physics with Cellular Automata // Ibid. P. 96–116.

9. *Creutz M.* Quarks, Gluons and Lattices. Cambridge: Cambridge University Press, 1983.

10. *Feynman R. P.* Statistical Mechanics. A Set of Lectures. Massachusetts: Benjamin, Inc., 1972.

11. *Soldatov S.* PLATO: Determination of Fractal Dimension: Diploma Thesis. Dubna: JINR, 2000.

12. *Qichang Li et al.* BIP: Biofilm Image Processing. University of Memphis, 2000; http://www.msci.memphis.edu/ giri/BIP/

13. *Ligget T. M.* Interacting Particle System. Springer-Verlag, 1985.

14. *Matzke Hj., Spino J.* Formation of the Rim Structure in High Burnup Fuel // J. Nucl. Materials. 1997. V. 248. P. 170–179.

15. *Matzke Hj., Kinoshita M.* Polygonization and High Burnup Structures in Nuclear Fuels // Ibid. V. 247. P. 108–115.

16. *Spino J., Vennix K., Coquerelle M.* Detailed Characterization of the Rim Microstructure in PWR Fuels in the Burn-up Range 40–67 GWd/tM // J. Nucl. Materials. 1996. V. 231. P. 179–190.